Supplementary Information

Imaging magnetic order in a two-dimensional iron-rich phyllosilicate

September 16, 2025

Muhammad Zubair Khan[1‡], Andriani Vervelaki[2‡], Daniel Jetter[2‡], Kousik Bagani[2‡], Andreas Ney[3], Oleg E.Piel[4], Sergio Valencia[5], Alevtina Smekhova[5], Florian Kronast[5], Daniel Knez [6], Martina Dienstleder [7], Martino Poggio[2,8*], and Aleksandar Matković[1,*]

1 *Chair of Physics, Montanuniversität Leoben, 8700 Leoben, Austria*;
2 *Department of Physics, University of Basel, 4056 Basel, Switzerland*;
3 *Institut für Halbleiter-und Festkörperphysik, Johannes Kepler Universität, A-4040 Linz, Austria.*;
4 *Group of computational materials design, Materials Center Leoben Forschung GmBH, Leoben, Austria*;
5 *Department of Spin and Topology in Quantum Materials, Helmholtz-Zentrum Berlin, Berlin, Germany*;
6 *Institute of Electron Microscopy and Nanoanalysis, Graz University of Technology (NAWI Graz), 8010 Graz, Austria*;
7 *Graz Centre for Electron Microscopy, 8010 Graz, Austria*
8 *Swiss Nanoscience Institute, University of Basel, 4056 Basel, Switzerland*

‡ equal contribution
* martino.poggio@unibas.ch, aleksandar.matkovic@unileoben.ac.at

Table of content:

Supplementary Figure 1: Structure of mono-layer annite

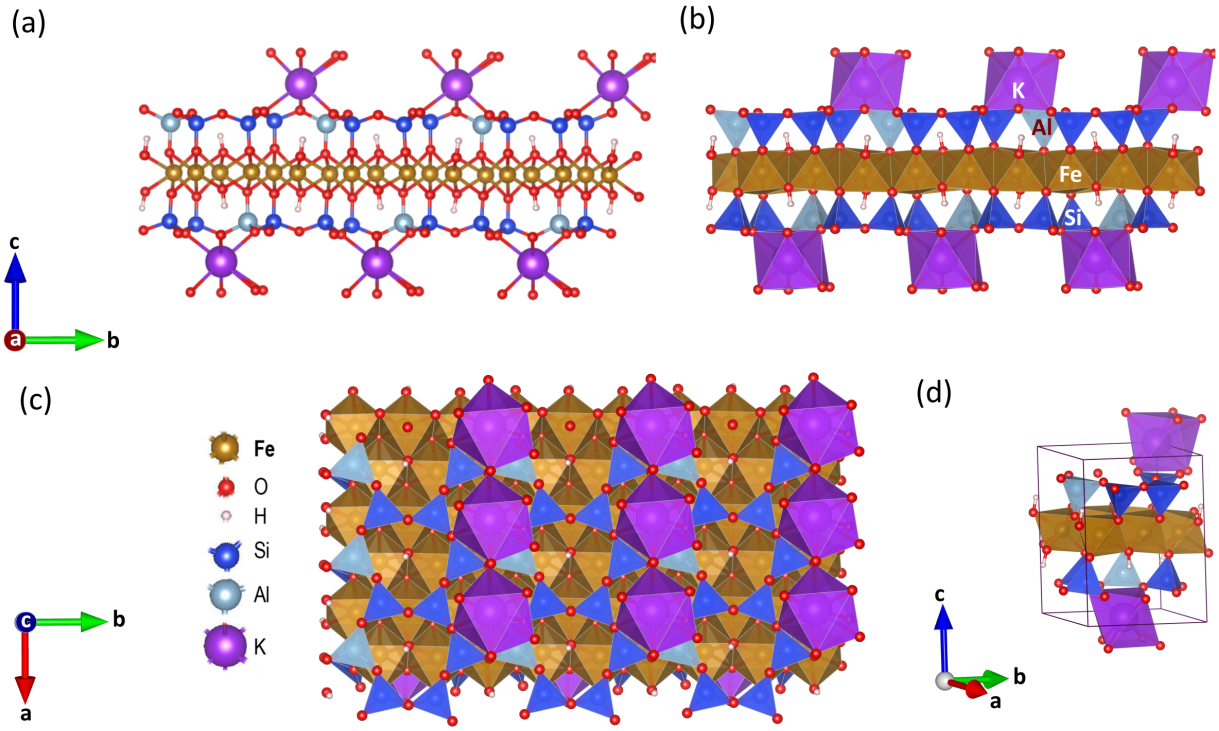

Supplementary Figure 1. Relaxed structure of annite monolayer obtained from ab-initio calculations: Side view in (a) ball-and-stick representation and (b) polyhedral representation. (c) Top view of the annite monolayer. (d) Unit cell of annite. Iron-centered octahedral units are shown in brown. Interlayer potassium ions (K) are represented as purple spheres. Tetrahedral groups containing silicon (Si) and aluminum (Al) are colored dark blue and light blue, respectively. Hydrogen (H) and oxygen (O) atoms are depicted as white and red spheres.

Supplementary Figure 2: Root mean square (rms) surface roughness and step height estimation

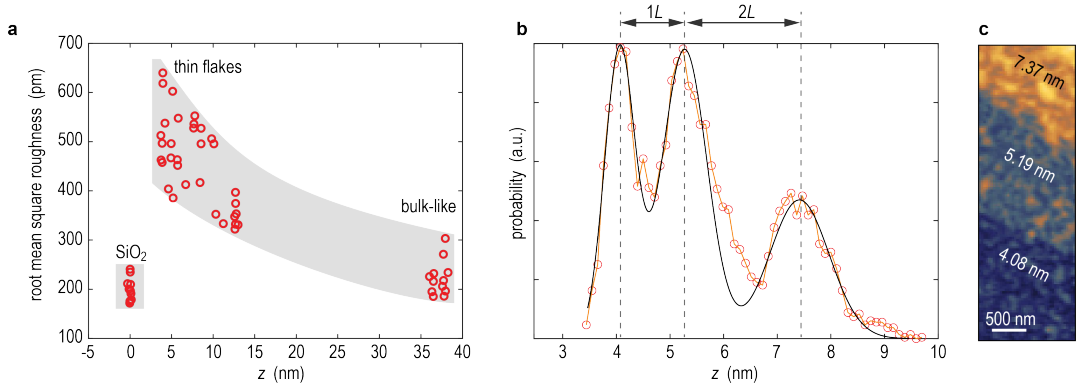

Supplementary Figure 2. Root mean square (rms) surface roughness and step height estimates: (a) rms roughness parameter extracted from 1x1 µm^2 flat terraces of the sample and the surrounding Si/SiO_2 substrate, shown as the function of the mean height value of the selected area (red circles). The shaded area indicates the trend and serves as a guide to the eye. A noticeable increase in roughness of over 2 times is observed between the thin flakes and the nearby substrate, which decreases with the increase in the flake thickness. (b) example on estimation of the number of monolayers of terrace from the peak fits to the histogram of the AFM topography image presented in (c). (c) AFM topography of a mono- and bi-layer step, 4x1.4 µm^2, z scale 9nm. The mean height of each terrace is indicated in the figure.

Supplementary Figure 3: Structural features: Confirmation of trapped impurities between flake and substrate

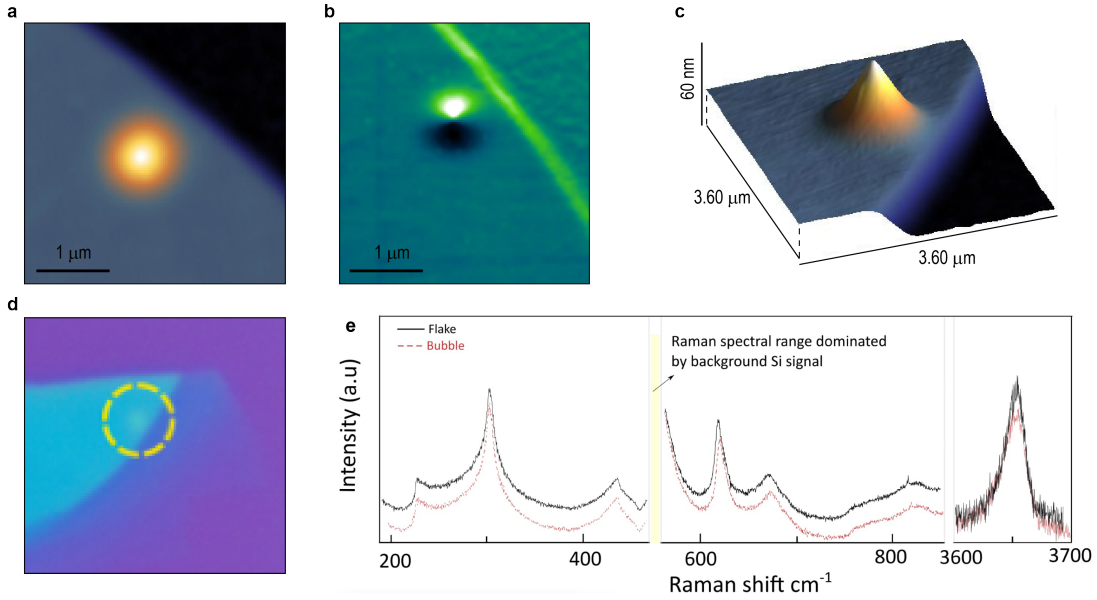

Supplementary Figure 3. Trapped impurities between the flakes and the substrate: (a) AFM topography and (b) phase images of annite flake,focusing on the trapped impurity between the flake and the Si/SiO_2 substrate (z scales respectively 60 nm and 30 deg). (c) 3D representation of the topography image from (a). (d) 12x12 µm^2 optical micrograph of the annite sample, dashed circle highlights the sample area presented in (a-c). (e) Raman spectra on the flat flake area near the "bubble" (black line) and on the bubble (red line), showing both lower wavenumber modes (200-850 cm^{-1}) and OH mode at 3700 cm^{-1}. c-Si peak of the substrate at 520 cm^{-1} has been cut out for more clear presentation of the samples' modes.

Supplementary Figure 4: Overview scanning SQUID microscopy maps with varied external in-plane field

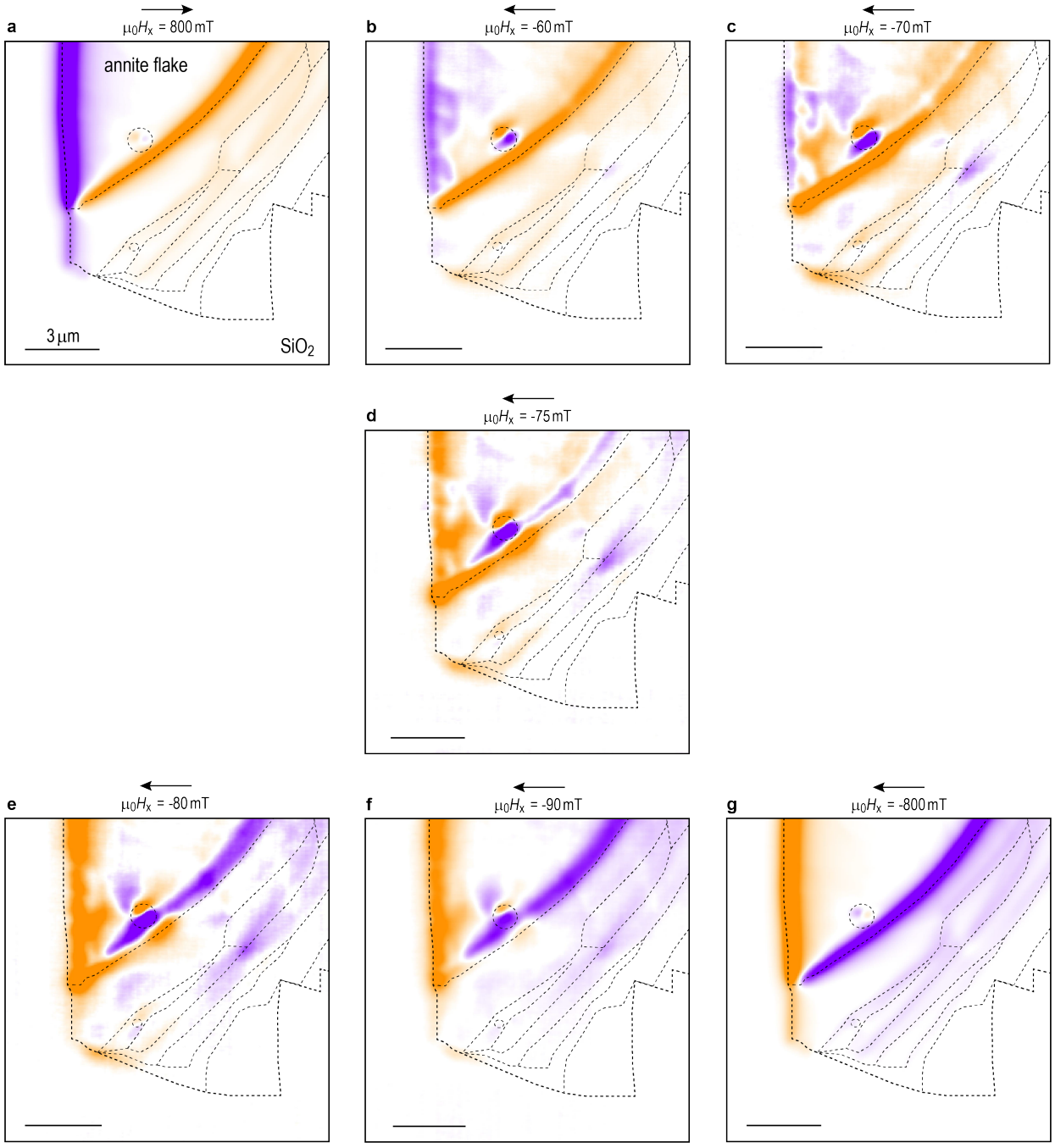

Supplementary Figure 4. Overview SSM maps with varied external in-plane field: Each panel presents a DC overview B_z^{avg} signal, dashed lines indicate correlation to the topographical edges of the sample with respect to Figure 1b-c of the main text. Applied external fields are indicated above each sub-panel, and the field sequence follows a down-sweep from 800 mT to -800 mT. The z ranges are set to better highlight the features, and are as following: **(a)** z range ±250 μT, **(b)** z range ±100 μT, **(c-e)** z range ±50 μT, **(f)** z range ±100 μT, **(g)** z range ±250 μT,

Supplementary Figure 5: Additional statistics for the $M(H)$ hysteresis loop parameters

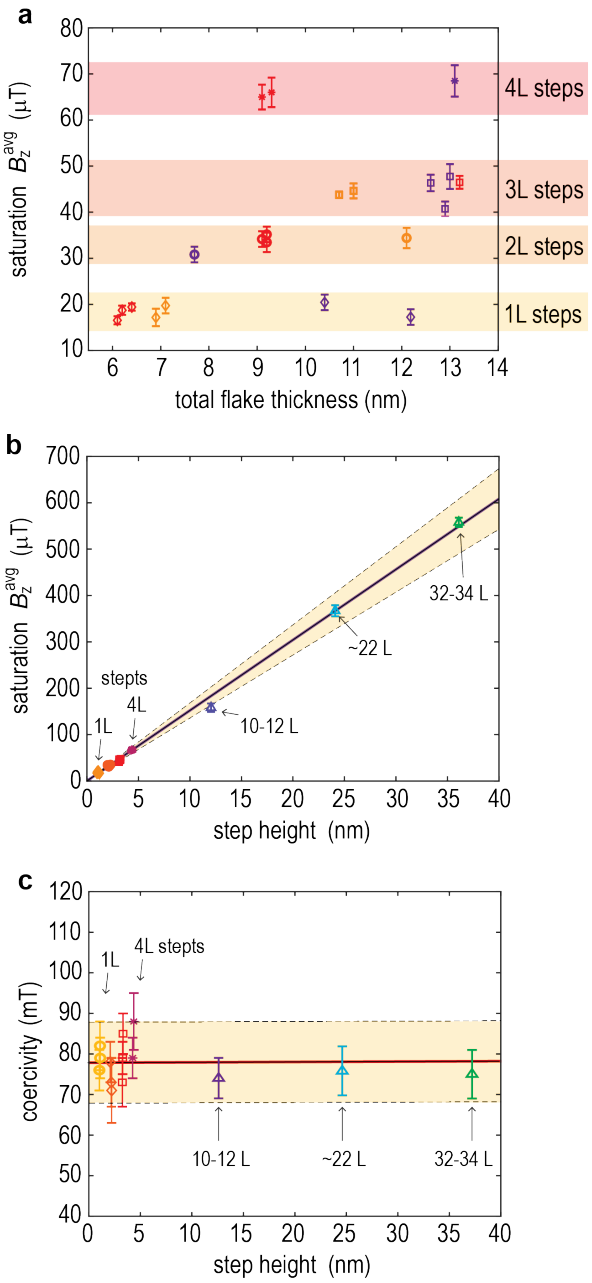

Supplementary Figure 5. Additional statistics for the $M(H)$ hysteresis loop parameters: (a) Saturation of the magnetization, extracted at 800 mT of the in-plane applied external field, as a function of the total layer thickness, considering the height of the upper edges of the terraces. Colors indicate different SSM maps (different sample regions), diamonds indicate 1L steps, circles 2L steps, squares 3L steps and stars 4L steps, as also highlighted by the shaded areas. The same data is plotted in Figure 2a in the main text as a function of the step height. Here the lack of correlation to the total flake height highlights that in the saturation the layers below the step edge do not contribute to the signal. **(b)** Saturation of the magnetization as the function of the step height including the data for bulk-like (over 10 nm) step edges. **(c)** Coercivity as the function of the step height including the data for bulk-like (over 10 nm) step edges. Error bars in (a) and (c) demonstrate the standard deviation, as measurements performed on multiple spots along the steps.

Supplementary Figure 6: Low signal observed for sub-5 nm thick regions

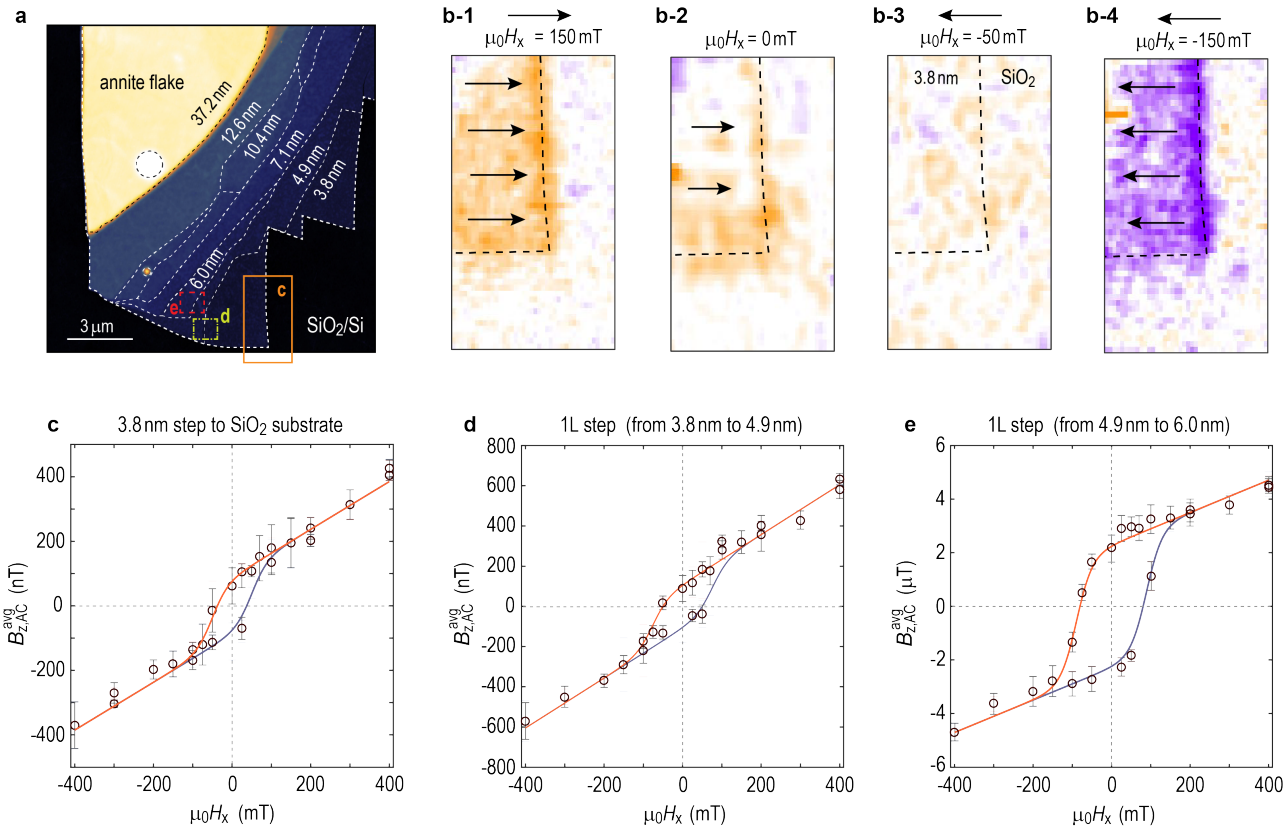

Supplementary Figure 6. Low signal observed for sub-5 nm thick regions: **(a)** AFM topography overview (also in Figure 1c), with highlighted rectangles focusing on the hysteresis reconstruction in the thin region of the sample. Solid orange rectangle highlighted in (a) focuses on the step edge to the SiO_2 substrate with the total flake height of 3.8 nm. Further data from this region is presented in (b1-b4) and (c). Dot-dashed yellow rectangle in (a) focuses on a 1L step from 3.8 nm to 4.9 nm and its corresponding hysteresis is presented in (d), and as a reference the data extracted from the dashed red rectangle region highlighted in (a) focuses on the subsequent 1L step, and is presented in (e). **(b1-4)** Downwards field sweep SOL maps for the flake edge, externally applied in-plane filed in x direction of the scanner is noted above each panel. Solid arrows indicate the direction of the magnetization in the film, dashed lines indicate the edge of the sample, dashed circles indicate bubbles in the film. **(c)** Reconstructed hysteresis loop for the thin edge of the sample. **(d)** Reconstructed hysteresis loop for the first 1L step. **(e)** Reconstructed hysteresis loop for the second 1L step. Error bars in (c-e) demonstrate the standard deviation, as measurements performed on multiple spots along the steps. All data presented in (b-e) was recorded in the AC mode with the same lift parameters. Only after about 5 nm of the total flake thickness, consistent and comparable response was observed, while the signal in the thin region was found to be about 20 times lower. A likely explanation for this is interaction with the SiO_2 substrate. It could be possible that trapped charges in SiO_2 or at the annite/SiO_2 interface introduce transition of Fe ions from 2+ to 3+ state, leading to a predominantly paramagnetic response.

Supplementary Figure 7: Additional FC and ZFC SSM maps for bi-layer and 4 layer steps

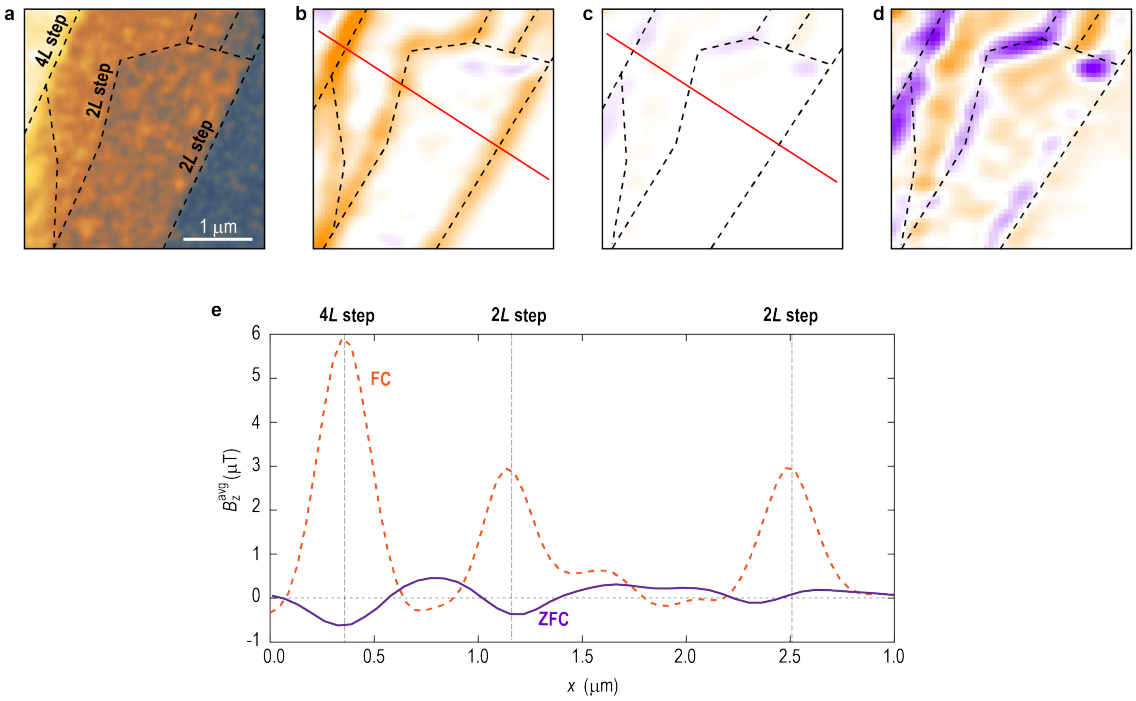

Supplementary Figure 7. Additional ZFC and FC SSM maps for even number of monolayer steps: (a) topography of the sample region featuring several even numbered monolayer terraces (z scale 20nm). Dashed lines highlight the step edges, in both topography and the SSM maps of the same area (b-d). (b) FC SSM map (z scale +5). (c) the same region as is (b) only under ZFC conditions (same scale bar for comparison). (d) ZFC map from (c) with 10x reduced scale to highlight the relation of the features to the topography (z scale +0.5). (e) Cross-sections of the B_z^{avg} signal from the FC (orange dashed line) and ZFC (solid purple line) conditions; marked by the red line in (b,c).

Supplementary Figure 8: SSM map of a thicker region of the sample under ZFC conditions, with highlighted domains

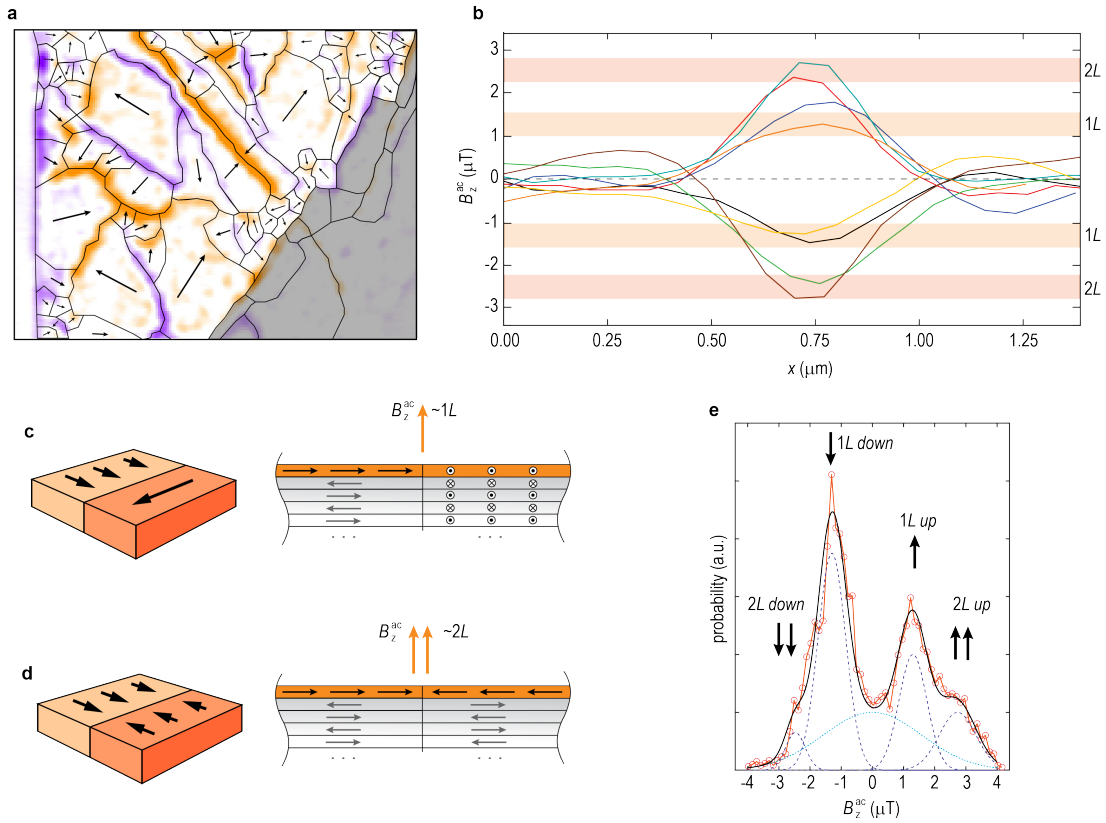

Supplementary Figure 8. Domains in the SSM ZFC map of the bulk-like region: (a) Repeated area from Figure 3(g), with the lines illustrating a possible configuration of the magnetic domains, assuming that the out of plane field detected by the SSM arises from the wall of the AFM ordered regions with opposite layer polarization. Arrows illustrate the likely direction of the domain polarization. The shaded area marks the thin region of the flake, 10x8μm^2 area, z scale +2 T. (b) eight cross-sectional lines from (a). Shaded yellow and orange areas indicate the signal that is corresponding to a 1L and 2L steps from FC measurements in comparable conditions. (c,d) illustrate how the signal intensity of the two domain edges would be expected to vary from the equivalent to a one uncompensated monolayer (c - domains orthogonally polarized) to a maximum of two uncompensated monolayers (d - domains antiparallelly polarised). (e) histogram (red circles) of the field intensities from (a) and the Gaussian fit (solid black line cumulative, dashed lines individual peaks).

Supplementary Figure 9: Additional bulk SQUID magnetometry data on parasitic paramagnetic contribution

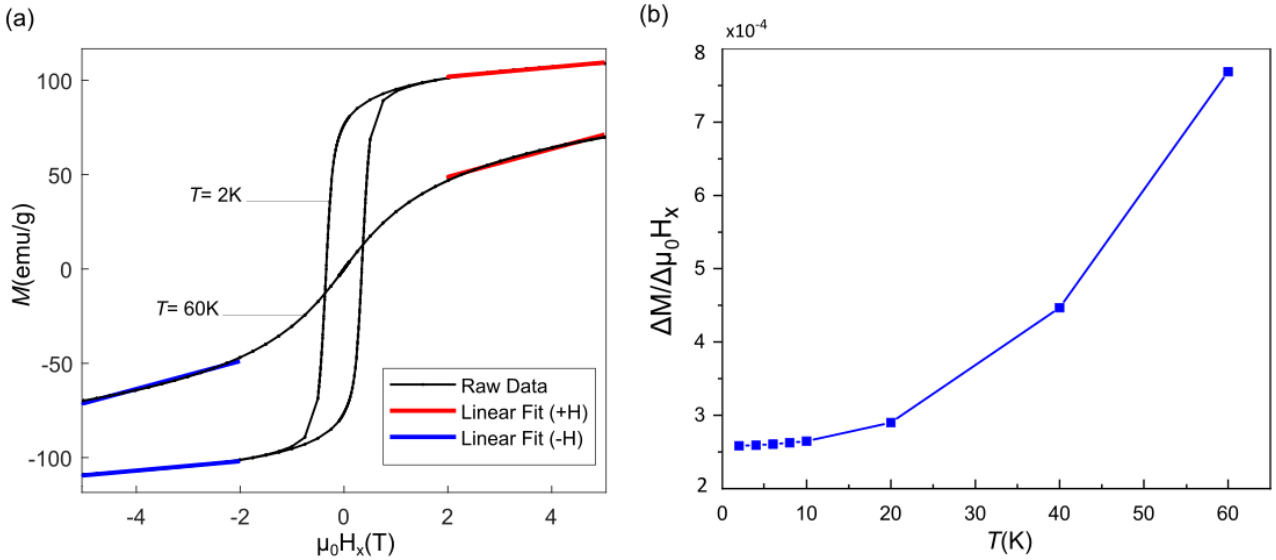

Supplementary Figure 9. Parasitic paramagnetic contribution: (a) $M(H)$ Hysteresis loops (at 2 K and 60 K) of a bulk single-crystal annite recorded in in-plane configuration. Red and blue solid lines indicate the linear fit to paramagnetic slope. (b) Paramagnetic contribution as a function of temperature. At higher temperature, the parasitic paramagnetic signal appears to be no longer distinguishable from main paramagnetic response of the system.

Supplementary Figure 10: Additional bulk SQUID magnetometry data on out-of-plane response

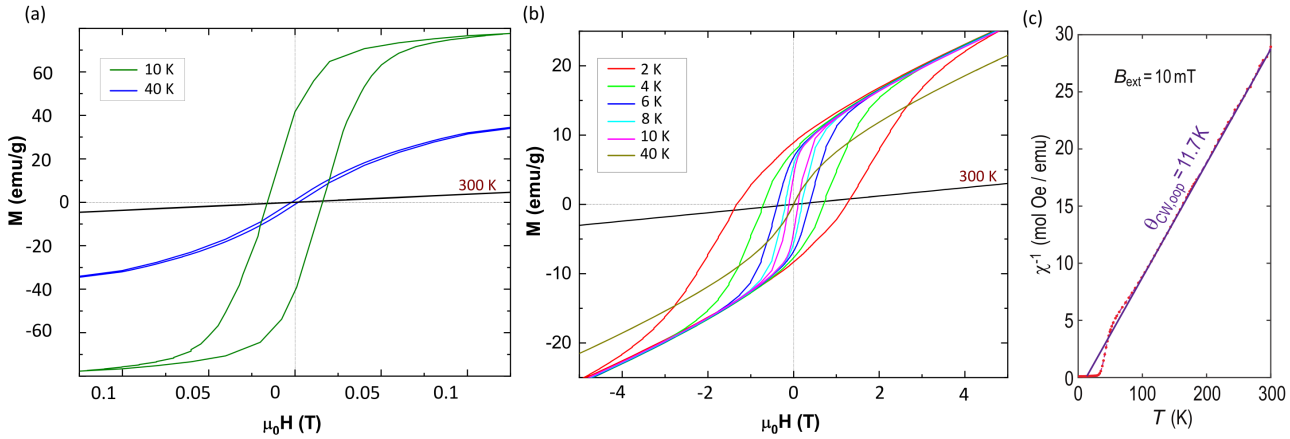

Supplementary Figure 10. Additional bulk SQUID magnetometry data on out-of-plane response: (a,b) $M(H)$ hysteresis loops in the case of the out-of-plane applied external field. (a) Comparing the data obtained at 10 K, 40 K, and 300 K, showing a transition from ferromagnetic to paramagnetic response. Note that at 40 K small hysteresis is still visible. (b) Evolution of the hysteresis between 2 K and 10 K. As a reference 40 K and 300 K data is also presented. In comparison to (a) a full field-sweep range of ±5 T is shown. **(c)** Inverse of the susceptibility as a function of the temperature obtained from the oop field-cooling measurements. Solid line represents the fit with respect to Curie-Weiss law (to the data from 100 K and above). Extracted θ_{CW} is indicated above the curve. The extraction of θ_{CW} is rather sensitive to the selected temperature range for the fit, as it can be clearly seen that below 100 K a more complex behavior is present.

Supplementary Figure 11: Additional bulk SQUID magnetometry data on Neel temperature

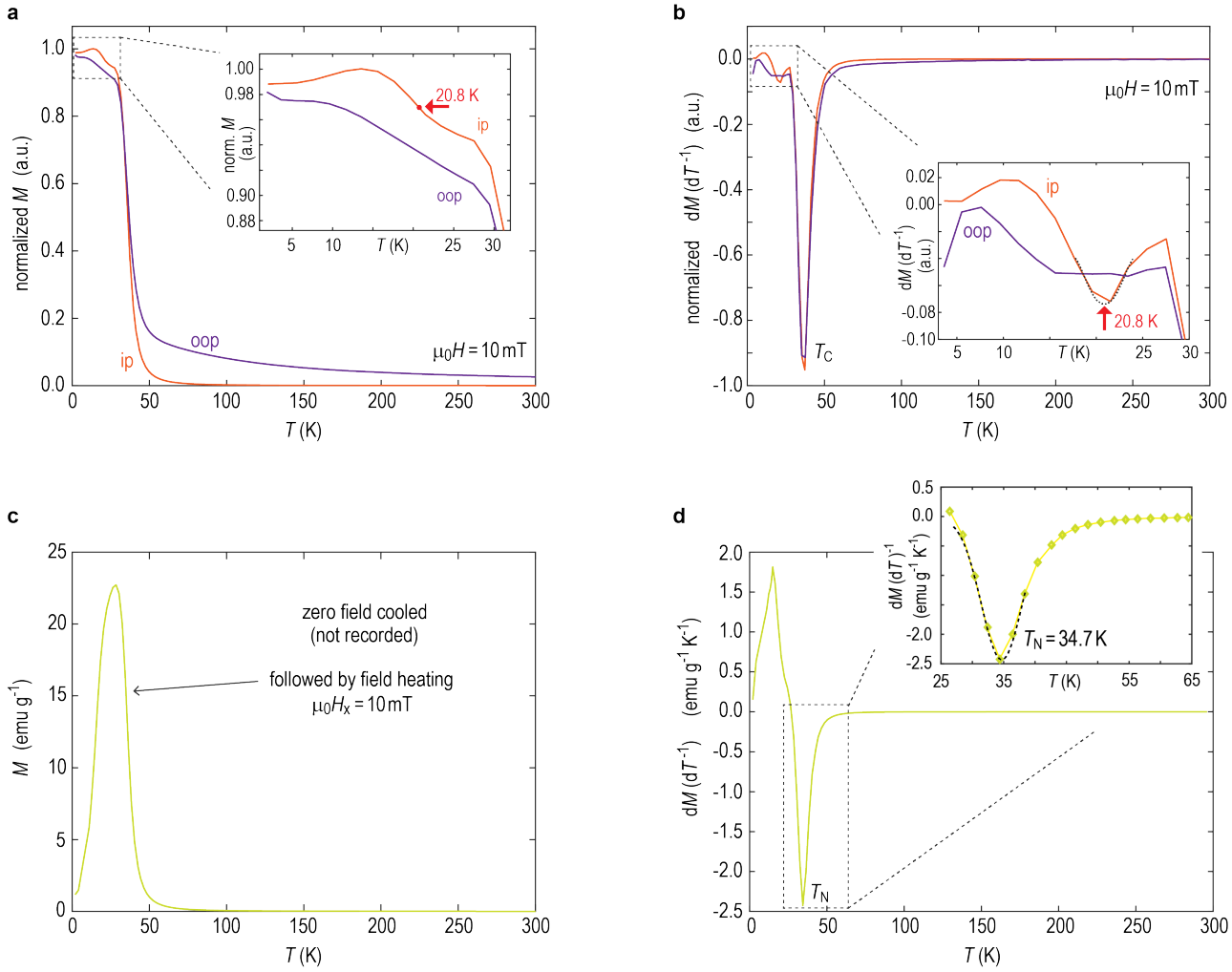

Supplementary Figure 11. Additional information on M(T) curves of the bulk sample: (a) M(T) curves for the field cooling (FC) case. The values for specific magnetization have been normalized for comparison. The ip curve is scaled by a factor of 0.04, while the oop curve is scaled by a factor of 4. The inset focuses on the region below 30 K. The second transition, which is prominent only in the ip case, is highlighted by a red arrow. (b) the temperature derivative of the curves presented in (a). The inset of (b) also focuses on the range below 30 K. The dotted black line in inset of (b) represents the fit to the local minima in the dM/dT ip FC curve, found to be at 20.8 K. (c) Zero field cooling (ZFC) M(T) curve for the full temperature range. The sample was cooled from 300 K in ZFC condition to the lowest achievable temperature, and then heated in 10 mT ip external field during the recording of the curve. (d) Temperature derivative of the curve from (c) with the global minima corresponding to the Néel temperature of the sample (TN), observed at 34.7 K. The inset of (d) focuses on the global minima in the dM/dT ZFC curve. Dotted black line represents a Gaussian fit in the minimum vicinity used to estimate the TN.

Supplementary Figure 12: Additional XAS data

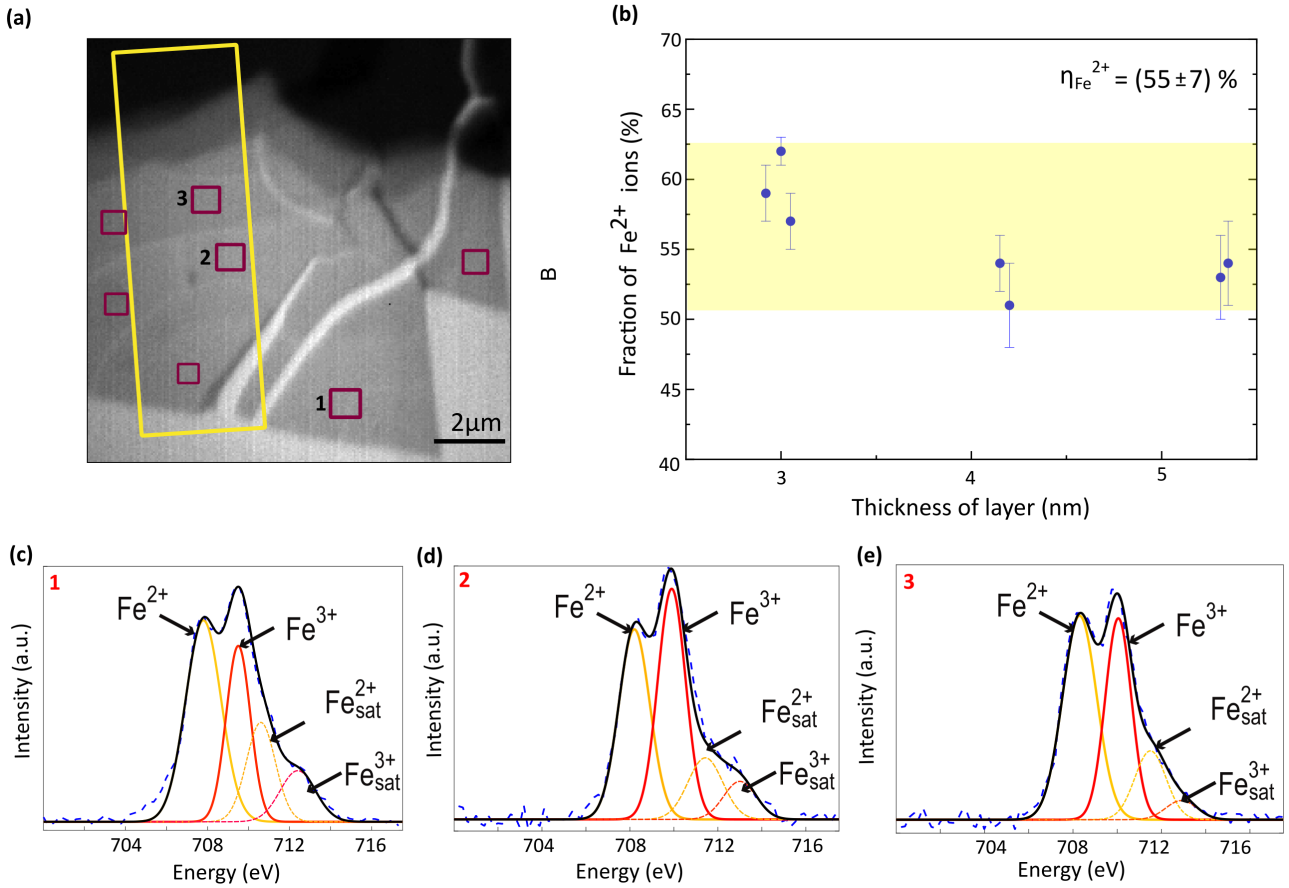

Supplementary Figure 12. Additional thickness-dependent XAS data: **(a)** XAS image of an annite flake on Au coated Si substrate, recorded in SPEEM configuration at 709 eV energy. Purple squares indicate regions of interest (ROIs), from which the XAS spectra was extracted. These regions are set on three teraces, with total thickness of 3.0 nm, 4.2 nm, and 5.3 nm. Yellow ROI indicates the region shown in the main manuscript Figure 4f. **(b)** Fraction of Fe^{2+} ions with respect to the total ($Fe^{2+} + Fe^{3+}$), extracted from fitting of the $L3$ edge XAS data, as a function of the layer thickness. The data indicates that iron is present in a mixed valence state throughout the entire flake, with the fraction of Fe^{2+} at (55 ± 7) % within the annite matrix, and without a strong connection of the valence state to the layer thickness in a thin region of the sample.Error bars demonstrate the standard deviation in the fraction of Fe^{2+} with respect to fitting of raw data. Thicker region was not possible to probe in a SPEEM configuration due to a lack of scattered electron signal. **(c-e)** Respectively, examples of the spectra and the fits from three ROIs, indicated in (a) with "1"-"3". The spectra present the Fe L_3 edge (dotted line) with individual Gaussian fits for the main and the satellite peaks that correspond to the 2+ and 3+ oxidation states of Fe. A cumulative fit is presented by the black line.